

# Simultaneous X-ray and gamma-ray observations of Cyg X-1 in the hard state by Ginga and OSSE

Marek Gierliński<sup>1,2</sup>, Andrzej A. Zdziarski<sup>2,3</sup>, Chris Done<sup>4</sup>, W. Neil Johnson<sup>5</sup>, Ken Ebisawa<sup>3</sup>, Yoshihiro Ueda<sup>6</sup>, Francesco Haardt<sup>7</sup>, and Bernard F. Phillips<sup>8,5</sup>

<sup>1</sup>*Astronomical Observatory, Jagiellonian University, Orla 171, 30-244 Cracow, Poland*

<sup>2</sup>*N. Copernicus Astronomical Center, Bartycka 18, 00-716 Warsaw, Poland*

<sup>3</sup>*Laboratory for High Energy Astrophysics, NASA/Goddard Space Flight Center, Greenbelt, MD 20771, USA*

<sup>4</sup>*Department of Physics, University of Durham, Durham DH1 3LE, UK*

<sup>5</sup>*E. O. Hulbert Center for Space Research, Naval Research Laboratory, Washington, DC 20375, USA*

<sup>6</sup>*Institute of Space & Astronautical Science, 3-1-1, Yoshinodai, Sagamihara-shi, Kanagawa 229, Japan*

<sup>7</sup>*Department of Astronomy & Astrophysics, Gothenburg University, 41296 Gothenburg, Sweden*

<sup>8</sup>*Universities Space Research Association, Washington DC 20024, USA*

Accepted 1997 February 10, Received 1996 October 15

## ABSTRACT

We present four X-ray/γ-ray spectra of Cyg X-1 observed in the hard ('low') state simultaneously by *Ginga* and *GRO* OSSE on 1991 June 6. The four spectra have almost identical spectral form but vary in the normalisation within a factor of two. The 3–30 keV *Ginga* spectra are well represented by power laws with an energy spectral index of  $\alpha \sim 0.6$  and a Compton reflection component including a fluorescent Fe K $\alpha$  corresponding to the solid angle of the reflector of  $\sim 0.3 \times 2\pi$ . These spectra join smoothly on to the OSSE range ( $\geq 50$  keV) and are then cut off above  $\sim 150$  keV. The overall spectra can be modelled by repeated Compton scattering in a mildly-relativistic, thermal plasma with the optical depth of  $\tau \sim 1$ . However, the high-energy cutoff is steeper than that due to single-temperature thermal Comptonisation. It can be described by a superposition of dominant  $\tau \sim 1$ –2, thermal emission at  $kT \sim 100$  keV and a Wien-like component from an optically-thick plasma at  $kT \sim 50$  keV.

The X-ray spectra do not show the presence of an anisotropy break required if thermal Compton scattering takes place in a corona above a cold disc. Also, the flat spectral index shows that the plasma is soft-photon starved, i.e., the luminosity in incident soft X-ray seed photons is very much less than that in the hard X-rays. Furthermore, the observed solid angle of the reflector is significantly less than  $2\pi$ . These facts taken together strongly rule out a disc-corona geometry. Rather, the observed spectra are consistent with a geometry in which the cold accretion disc (which both supplies the seed soft X-rays and reflects hard X-rays) only exists at large radii, while the Comptonising hot plasma is located in an inner region with no cold disc. This hot plasma consists of either pure  $e^\pm$  pairs if the source size is  $\sim 5$  Schwarzschild radii or it contains also protons if the size is larger.

**Key words:** accretion, accretion discs – gamma-rays: observations – gamma-rays: theory – stars: individual (Cygnus X-1) – X-rays: stars

## 1 INTRODUCTION

Cyg X-1, one of the brightest X-ray sources in the sky, was discovered in X-rays more than 30 years ago (Bowyer et al. 1965). This binary system is at a distance of  $\sim 2.5$  kpc and consists of the O9.7 Iab type supergiant HDE 226868 (Gies & Bolton 1986) orbiting around a compact object with a period of 5.6 days. The mass of the unseen companion is significantly larger than  $5 M_\odot$  (Dolan 1992), strongly sug-

gesting that it is a black hole. Focused wind accretion (Gies & Bolton 1986) from the primary star (which is extremely close to filling its Roche lobe) drives the powerful source of the X-ray radiation. The X-ray emission of Cyg X-1 exhibits strong variability on all time scales from milliseconds to months (e.g. Miyamoto & Kitamoto 1989; Priedhorsky, Terrel & Holt 1983). However, it spends most of the time in the hard (so-called 'low') X-ray state, characterised by a low flux in soft X-rays and strong hard X-ray and soft γ-ray

fluxes (e.g., Phillips et al. 1996, hereafter P96). In this state, the 50 keV flux changes by about an order of magnitude but the spectral variability is modest (P96). From time to time, Cyg X-1 is in the soft ('high') state (e.g., Liang & Nolan 1984, Cui et al. 1997), with a strong soft X-ray emission and a relatively weak tail in hard X-rays.

The hard-state spectrum of Cyg X-1 at  $\gtrsim 3$  keV consists typically of a power law with an energy spectral index of  $\alpha \sim 0.6$ –0.7 and a Compton-reflection continuum component, prominent above 10 keV (Done et al. 1992; Ebisawa et al. 1996, hereafter E96). This component also includes an Fe K edge above  $\sim 7$  keV and an Fe K $\alpha$  fluorescence line (Barr, White & Page 1985; Marshall et al. 1993; E96). The results of BBXRT (Marshall et al. 1993) and *ASCA* (E96) indicate that the line is narrow, with the width of  $\sigma \lesssim 0.2$  keV, suggesting its origin in outer parts of an accretion disc. The edge energy suggests the reflecting surface is mildly ionised, with Fe XI as the most abundant Fe species (E96).

The soft  $\gamma$ -ray spectra of Cyg X-1 in the hard state are steeply cut off above  $\sim 150$  keV (P96). P96 obtained good fits to the *GRO* OSSE spectra of Cyg X-1 with exponentially cut off power laws. However, the X-ray spectral index implied by those fits is much harder than that observed in X-rays, showing that the broad-band X-ray/ $\gamma$ -ray (hereafter  $X\gamma$ ) spectrum is more complex.

The most likely physical process responsible for the intrinsic continuum appears to be thermal Comptonisation of soft X-rays from thermal emission of a cold accretion disc at a temperature of  $\sim 100$  eV (e.g., Balucińska-Church et al. 1995). Haardt et al. (1993) pointed out that Comptonisation may take place in an optically thin plasma rather than in an optically thick one (as fitted by, e.g., Sunyaev & Trümper 1979).

In this work, we present four 2–1000 keV spectra of Cyg X-1 observed in the hard state simultaneously by *Ginga* and OSSE on 1991 June 6. This provides us with an unprecedented opportunity to study physical processes taking place in the  $X\gamma$  source as well as the source geometry. We consider thermal and nonthermal Comptonisation, Compton reflection,  $e^\pm$  pair production, and constraints on the sizes and relative covering factors of the  $X\gamma$  source and cold matter.

## 2 THE DATA

Cyg X-1 was observed four times by *Ginga* on 1991 June 6 during the OSSE viewing period 2 (P96). Overlapping observation periods provide us with four sets of nearly simultaneous data. The orbital phase during the four observations was from 0.70 to 0.85. Table 1 gives the log of observations. We adopt  $4661 \text{ cm}^2$  as the *Ginga* effective area, which is the standard value used in the Leicester data base (D. Smith, private communication). The high voltage of the *Ginga* LAC detector (Turner et al. 1989) was reduced in this observation, which lead to a usable energy range of 2–30 keV (E96). A 1 per cent systematic error was included in each *Ginga* channel.

The OSSE data are from 50 keV to 1000 keV. They include estimated systematic errors computed from the uncertainties in the low energy calibration and response of the detectors using both in-orbit and prelaunch calibration data. The energy-dependent systematic errors are expressed as an

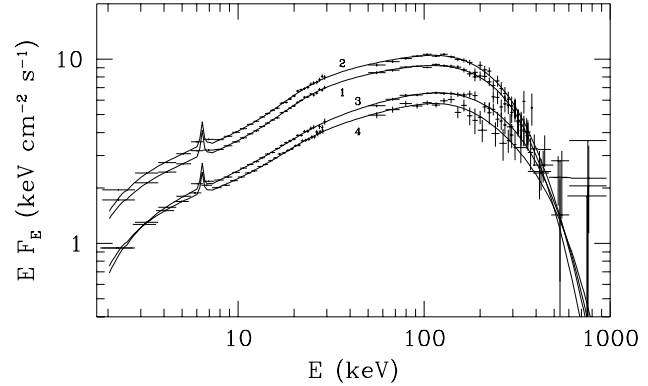


**Figure 1.** The four spectra of Cyg X-1, labelled by the observation number (see Table 1), observed simultaneously by *Ginga* and OSSE on 1991 June 6. The solid curves represent the two-temperature model described in Section 3.1. The data have been rebinned for clarity of the display.

uncertainty in the effective area in the OSSE response. These systematic errors were added in quadrature to the statistical errors. The former are most important at the lowest energies (approximately 3% uncertainty in effective area at 50 keV, decreasing to 0.3% at 150 keV and above).

Figure 1 shows the four unfolded spectra corresponding to the four data sets. (The solid curves represent a two-component model described in Section 3.1 below.) The ratio of the highest 2–1000 keV model flux to the lowest one, obtained during the second and the fourth observation, respectively (separated by about 15 hours), is  $\sim 1.8$ .

## 3 RESULTS

### 3.1 Spectral fits

In our fits, we use the XSPEC spectral fitting package version 9 (Arnaud 1996). Our model spectra are absorbed by a column density,  $N_{\text{H}}$ , which we constrain to be  $\geq$  the Galactic column,  $6 \pm 2 \times 10^{21} \text{ cm}^{-2}$  (Balucińska-Church et al. 1995). We obtain absorption larger than the Galactic one for some models, especially for the data sets 3 and 4 (Tables 2 and 3), which can be attributed to transient dips associated with the intervening gas (Kitamoto et al. 1984). In X-rays, the spectra consist clearly of two components: an underlying power law and a component due to reflection from the surface of an accretion disc including both continuum Compton reflection and a fluorescent Fe K $\alpha$  line (e.g., George & Fabian 1991).

We first fit the *Ginga* data only with the incident continuum in the form of a power law e-folded with  $E_c = 300$  keV together with the Compton reflection component and an iron line. In the spectral fitting we ignore the data below 3 keV due to the presence of a soft excess at lower energies (E96), but we show these data in the plots (Figs. 1–4). We use angle-dependent Compton reflection Green's functions of Magdziarz & Zdziarski (1995). The disc inclination is assumed to be less than  $67^\circ$  (Dolan & Tapia 1989), and in most fits the most probably inclination of  $30^\circ$  is used (Gies & Bolton 1986). The luminosity intercepted by the reflecting medium equals  $\Omega/2\pi$  times the luminosity emitted outward

**Table 1.** The log of observations in UT on 1991 June 6. The counts of *Ginga* and OSSE are for 2–30 keV and 50–150 keV, respectively.

Data set	<i>Ginga</i>			OSSE				
	Start	End	Live time [s]	Counts/s	Start	End	Live time [s]	Counts/s
1	00 <sup>h</sup> 17 <sup>m</sup> 50 <sup>s</sup>	02 <sup>h</sup> 09 <sup>m</sup> 50 <sup>s</sup>	2304	3410 ± 10	00 <sup>h</sup> 02 <sup>m</sup> 32 <sup>s</sup>	00 <sup>h</sup> 37 <sup>m</sup> 29 <sup>s</sup>	1806	455 ± 4
2	04 <sup>h</sup> 43 <sup>m</sup> 26 <sup>s</sup>	06 <sup>h</sup> 29 <sup>m</sup> 02 <sup>s</sup>	888	3890 ± 10	01 <sup>h</sup> 23 <sup>m</sup> 21 <sup>s</sup>	02 <sup>h</sup> 11 <sup>m</sup> 09 <sup>s</sup>	2315	554 ± 4
3	11 <sup>h</sup> 02 <sup>m</sup> 38 <sup>s</sup>	14 <sup>h</sup> 24 <sup>m</sup> 46 <sup>s</sup>	2828	2290 ± 10	04 <sup>h</sup> 28 <sup>m</sup> 46 <sup>s</sup>	05 <sup>h</sup> 03 <sup>m</sup> 43 <sup>s</sup>	1741	456 ± 5
					06 <sup>h</sup> 02 <sup>m</sup> 26 <sup>s</sup>	06 <sup>h</sup> 50 <sup>m</sup> 29 <sup>s</sup>	2299	665 ± 5
					10 <sup>h</sup> 42 <sup>m</sup> 50 <sup>s</sup>	11 <sup>h</sup> 15 <sup>m</sup> 36 <sup>s</sup>	1708	400 ± 4
					12 <sup>h</sup> 14 <sup>m</sup> 47 <sup>s</sup>	12 <sup>h</sup> 54 <sup>m</sup> 07 <sup>s</sup>	2010	371 ± 4
					13 <sup>h</sup> 48 <sup>m</sup> 41 <sup>s</sup>	14 <sup>h</sup> 32 <sup>m</sup> 23 <sup>s</sup>	2257	307 ± 4
4	20 <sup>h</sup> 22 <sup>m</sup> 14 <sup>s</sup>	20 <sup>h</sup> 43 <sup>m</sup> 58 <sup>s</sup>	1272	2080 ± 10	20 <sup>h</sup> 02 <sup>m</sup> 15 <sup>s</sup>	20 <sup>h</sup> 32 <sup>m</sup> 50 <sup>s</sup>	1629	316 ± 4

by the  $X\gamma$  source, where  $\Omega$  is the solid angle subtended by the reflector as seen from the source of isotropic radiation. In some models, the reflecting medium is allowed to be ionised with an ionisation parameter,  $\xi = L/(nr^2)$ , where  $L$  is the 5 eV–20 keV luminosity in a power law spectrum and  $n$  is the density of the reflector located at distance  $r$  from the illuminating source (Done et al. 1992). The reflector temperature is kept at 130 eV, which corresponds to the temperature of the soft X-ray spectral component (Balucińska-Church et al. 1995). The abundances are from Anders & Ebihara (1982) except that the relative Fe abundance,  $A_{\text{Fe}}$ , is a free parameter. The ion edge energies and opacities are from Reilman & Manson (1979) except for the Fe K-edge energies taken from Kaastra & Mewe (1993).

We find little intrinsic spectral variability in the *Ginga* data, so we use the average *Ginga* spectrum to better constrain the parameters in X-rays. We obtain  $\alpha = 0.59^{+0.03}_{-0.03}$ ,  $\Omega/2\pi = 0.34^{+0.05}_{-0.05}$ ,  $A_{\text{Fe}} = 2.1^{+0.3}_{-0.3}$  ( $\chi^2 = 21/22$  d.o.f.). The ionisation of the reflector is weak,  $\xi = 23^{+26}_{-22}$  erg cm s<sup>-1</sup>. There is a distinct Fe K $\alpha$  line in the spectrum, which we model here as a Gaussian centred at 6.4 keV and with the width of 0.1 keV, consistent with both the *Ginga* resolution not allowing us to resolve the line and the *ASCA* results indicating the line is narrow (E96). The line equivalent width is  $\text{EW} = 74^{+26}_{-22}$  eV. These results are similar to those obtained for other *Ginga* observations (e.g. E96).

In the fits with both *Ginga* and OSSE below, we examine the effect of allowing the relative normalisation of the two data sets to be free within ±15 per cent (which is a conservative limit to the relative calibration uncertainty of the two instruments). However, we find the relative normalisation to be consistent with unity as allowing it to be free leads to marginal fit improvements only. Therefore, in tables and figures below we use the actual normalisation of the *Ginga* and OSSE spectra.

When we extrapolate the *Ginga* model to the OSSE range, there is a good match around 50 keV, but the OSSE data require a cutoff in the spectrum at  $\gtrsim 150$  keV. However, a simple e-folded power law together with its reflection spectrum gives a cutoff much too shallow to account for the sharp break seen in the data, e.g.,  $\chi^2_{\nu} = 220/76$  for the data set 2. (The best fit parameters for this data set are:  $\alpha = 0.52$ ,  $E_c = 270$  keV,  $\Omega/2\pi = 0.28$ .)

However, e-folded power laws approximate only roughly thermal Comptonisation spectra, as discussed by, e.g., Poutanen & Svensson (1996; hereafter PS96). Therefore, we then use a thermal-Compton disc-corona model of PS96. In the model used, the hot coronal plasma is assumed to

form hemispheres (with the radial Thomson optical depth of  $\tau$ ) on the surface of an accretion disc. This model, however, is also very strongly ruled out by the data, yielding  $\chi^2_{\nu} \sim 1000/75$ . The main reason for the bad fit is the presence of an *anisotropy break* in the underlying model spectrum. The anisotropy break appears in the disc-corona spectrum viewed from above (at  $i = 30^\circ$ ) around the peak energy of the second-order scattering because the first-order scattering is directed mainly towards the disc (Stern et al. 1995; PS96; Svensson 1996). For the seed blackbody photons at the temperature of 130 eV (Balucińska-Church et al. 1995) and the hot plasma temperature of  $\sim 100$  keV, the anisotropy break energy is  $\sim 6$  keV. The *Ginga* data are instead very well described by a *single* power law up to 30 keV and a Compton-reflection component on top of it, as found above. A secondary problem with the model of PS96 applied to the present data is the predicted solid angle of the reflector of  $\Omega = 2\pi$ , whereas the data prefer a lower value. Still, allowing  $\Omega < 2\pi$  in the model (which may correspond to a cold disc present only at a limited range of radii) does not result in an acceptable fit. E.g., the fit to the data set 1 (Fig. 2) yields  $\chi^2_{\nu} = 160/75$  for  $kT = 92$  keV,  $\tau = 2.2$ ,  $\Omega/2\pi = 0.24$  for  $i = 30^\circ$ . The model can be strongly ruled out ( $\chi^2 = 117$ ) even for the largest viewing angle allowed by the optical data,  $i = 67^\circ$  (Dolan & Tapia 1989). The reason for the bad fit of the corona model is still the presence of the anisotropy break in the incident model spectrum. E.g., the incident spectrum in Figure 2 (dashed curve) can be approximated by a harder power law,  $\alpha \simeq 0.43$ , below 5.8 keV and a softer one,  $\alpha \simeq 0.56$  above it. The pattern of residuals in Figure 2 clearly show how this broken power-law-like model does not fit the data (which are consistent with a *single* incident power law).

We have also considered the homogeneous disc-corona model of Haardt & Maraschi (1993) as a phenomenological description of the data (although that model does not satisfy the energy balance in the case of Cyg X-1, see Section 3.2). For that model, we use the code of Haardt (1993). The main difference with respect to the hemisphere model above is that now there is strong Comptonisation of the reflection component by the hot corona with  $\tau \sim 1$  above the disc (see, e.g., PS96). Again, no acceptable fit is obtained,  $\chi^2_{\nu} \sim 200/75$ . Thus, the spectral data of Cyg X-1 *rule out* the disc-corona model regardless of the corona geometry.

Motivated by our ruling out the disc-corona model, we have considered thermal Comptonisation in a hot plasma cloud irradiated approximately *isotropically* by soft seed photons. This removes the presence of the anisotropy break

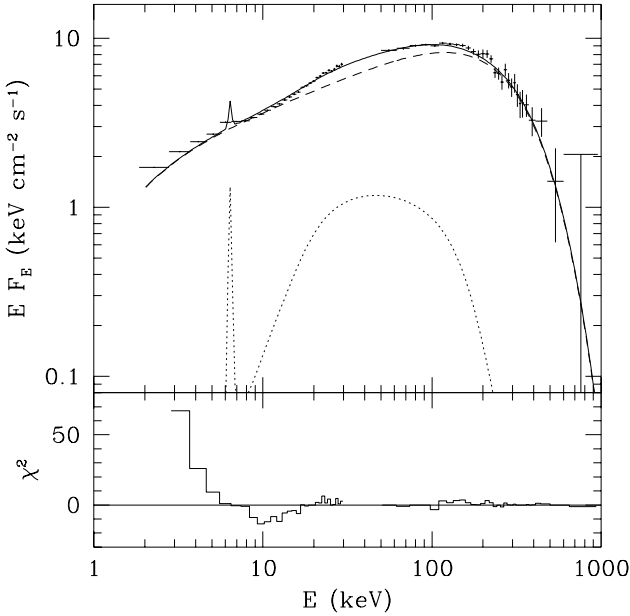


**Figure 2.** The anisotropic disc-corona model (PS96) fitted to the data set 1. The upper panel shows the data (crosses), the thermal Comptonisation continuum (dashed curve), and the reflection component (dotted curve). The solid curve shows the sum. The lower panel in this figure and in figures below shows the contribution to the total  $\chi^2$  from separate data channels [multiplied by the sign of (data – model)]. This model provides no satisfactory fit to the data due to the incident spectrum having a break at  $\sim 5$  keV.

in the spectrum, but it retains the proper description of the high-energy cutoff from Comptonisation. To this end, we used an isotropic-scattering version of the Comptonisation code of PS96 (J. Poutanen, private communication). We have assumed that a fraction of 0.3 of the reflection spectrum undergoes further thermal Comptonisation in the hot cloud, which is consistent with source geometry inferred from energy balance (Section 3.2 below); the fit results are insensitive to this number as long as it is  $\ll 1$ . Also, the fits are insensitive to the viewing angle; if  $i$  is increased from our default value of  $30^\circ$  to  $67^\circ$ ,  $\chi^2$  remains the same within  $\pm 1$  for the four data sets. This model does not allow the reflector to be ionised, which may result in some overestimate of  $\chi^2$  since the *Ginga* data indicate the reflector is weakly ionised. The Fe abundance of this model consistent with all 4 data sets is  $A_{\text{Fe}} = 1$ . As expected, we obtain a dramatic improvement of the fits, with  $\chi^2 \lesssim 1$  now. The fit results for the four data sets are given in Table 2, and the fit to the data set 2 is presented in Figure 3. We see that the hot plasma parameters are  $kT \simeq 100$  keV and  $\tau \simeq 2$  for all data sets.

We have tested the isotropic Comptonisation code of PS96 by our own Monte Carlo calculations (see Zdziarski, Johnson & Magdziarz 1996). We assumed a spherical source illuminated by seed photons at the center. We obtain the same plasma temperature,  $kT \simeq 100$  keV, but the radial optical depth of the sphere is  $\tau \simeq 1.3$ . The difference between this  $\tau$  and  $\tau \simeq 2$  obtained above is explained by the difference between the spherical source in the Monte Carlo

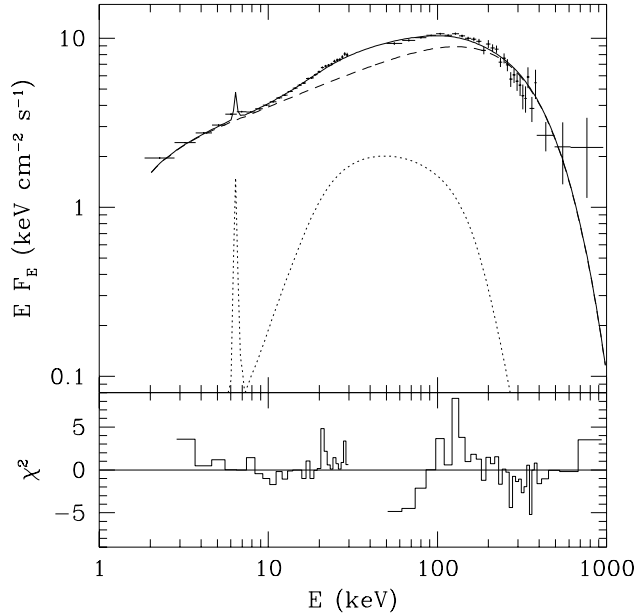


**Figure 3.** The isotropic one-temperature thermal Comptonisation model fitted to the data set 2. The upper panel shows the data (crosses), the thermal Comptonisation continuum (dashed curve) and the reflection component (dotted curve). The solid curve shows the sum. This model yields  $\chi^2_\nu < 1$ , but there is still a systematic residual pattern for the OSSE data (the lower panel).

calculations and the hemisphere source in the method of PS96.

Although  $\chi^2_\nu < 1$  for the isotropic Comptonisation model, there are still strong systematic residuals in the fit to the OSSE data, see the lower panel of Figure 3. Specifically, the model spectrum cuts off at high energies less than the data, i.e., the model spectrum is broader than the observed spectrum. Such an effect could appear if there were an additional narrow spectral component at high energies. Such a sharp spectral component can be due to a hot, optically-thick plasma component in the source, e.g., a transition region between the hot and the cold medium in the accretion flow (Misra & Melia 1996).

We have therefore considered models with two hot-plasma components. The first component, along with its reflection, is computed in the same way as in the isotropic Comptonisation model above. The Fe abundance is kept at  $A_{\text{Fe}} = 1.0$ , which is both the average value from fits to the four spectra and a value within the confidence limits of all of the four fits. The second, additional component (whose reflection is not considered) is due to optically-thick thermal Comptonisation and it is computed using a modified Kompaneets equation as in Zdziarski et al. (1996). We see in Table 3 and Figure 4 that addition of a second Comptonisation component with  $kT' \sim 50$  keV improves significantly the fit. In the actual fits, we have had to prevent the secondary component from giving a dominant contribution at low energies. This is achieved by fixing its low-energy spectral index to  $\alpha' = 0.15$ , which we found to have a negligible effect on  $\chi^2$ . The Thomson optical depth of the second plasma component has been found by the Monte Carlo method. It is  $\tau' \simeq 6$  for

**Table 2.** The parameters of the fits with the single-temperature isotropic model.  $I$  is the 1-keV normalisation in  $\text{cm}^{-2} \text{ s}^{-1}$ ,  $kT$  is in keV, and EW is in eV. The column density,  $N_{\text{H}}$  (in units of  $10^{22} \text{ cm}^{-2}$ ), is constrained to be  $\geq$  the lower limit on the Galactic column. The errors are given for 90 per cent confidence intervals,  $\Delta\chi^2 = 2.7$  (Lampton et al. 1976), and  $\chi^2$  is given for 76 d.o.f.

Obs.	$N_{\text{H}}$	$kT$	$\tau$	$\Omega/2\pi$	$I$	EW	$\chi^2$
1	$0.4^{+0.14}_{-0}$	$103^{+7}_{-5}$	$1.98^{+0.09}_{-0.12}$	$0.34^{+0.03}_{-0.03}$	1.19	$137^{+27}_{-29}$	69
2	$0.4^{+0.09}_{-0}$	$99^{+6}_{-5}$	$2.04^{+0.09}_{-0.11}$	$0.32^{+0.04}_{-0.03}$	1.34	$137^{+29}_{-28}$	97
3	$1.19^{+0.18}_{-0.17}$	$101^{+8}_{-8}$	$2.08^{+0.12}_{-0.13}$	$0.19^{+0.03}_{-0.03}$	0.79	$121^{+30}_{-29}$	60
4	$0.78^{+0.20}_{-0.21}$	$120^{+22}_{-16}$	$1.74^{+0.24}_{-0.27}$	$0.25^{+0.04}_{-0.04}$	0.74	$111^{+31}_{-32}$	64

**Table 3.** The parameters of the fits with the two-component thermal-Comptonisation model. The parameters of the main component are denoted by the same symbols as in Table 1, and  $I'$  and  $kT'$  are the 1-keV normalisation and temperature of the secondary component in units of  $\text{cm}^{-2} \text{ s}^{-1}$  and keV, respectively.  $L$  is the 2–1000 keV luminosity in  $10^{37} \text{ erg s}^{-1}$  for the assumed distance of 2.5 kpc, and  $\chi^2$  is given for 74 d.o.f.

Obs.	$N_{\text{H}}$	$kT$	$\tau$	$\Omega/2\pi$	$I$	$kT'$	$I'$	EW	$L$	$\chi^2$
1	$0.85^{+0.26}_{-0.27}$	$104^{+17}_{-17}$	$1.76^{+0.32}_{-0.26}$	$0.49^{+0.07}_{-0.07}$	1.33	$51^{+9}_{-7}$	0.0080	$115^{+31}_{-30}$	3.7	48
2	$0.95^{+0.27}_{-0.27}$	$107^{+19}_{-17}$	$1.67^{+0.29}_{-0.28}$	$0.53^{+0.07}_{-0.07}$	1.53	$47^{+6}_{-5}$	0.0106	$110^{+32}_{-33}$	4.1	64
3	$1.50^{+0.29}_{-0.30}$	$108^{+14}_{-15}$	$1.87^{+0.17}_{-0.24}$	$0.25^{+0.06}_{-0.05}$	0.83	$43^{+21}_{-13}$	0.0026	$104^{+32}_{-28}$	2.6	56
4	$1.18^{+0.28}_{-0.28}$	$127^{+27}_{-23}$	$1.53^{+0.30}_{-0.28}$	$0.32^{+0.08}_{-0.06}$	0.79	$36^{+13}_{-10}$	0.0042	$87^{+32}_{-35}$	2.3	54

a sphere with a central source of seed photons. The luminosity in the best-fit optically-thick component is 13, 15, 5, and 8 per cent of the total luminosity for the data sets 1, 2, 3, and 4, respectively. This model provides excellent fits to the data ( $\chi^2 \sim 50$ –60/74 d.o.f.), and the improvement with respect to the one-temperature model is statistically significant at more than 99.9 per cent (the probability that the reduction of  $\chi^2$  is by chance is  $\simeq 10^{-13}$ ) taking into account all four data sets. The two-component model strongly favours a face-on geometry; when  $i$  is increased from  $30^\circ$  (assumed above) to  $i = 67^\circ$ ,  $\Delta\chi^2 \simeq +7$  for each of the data set 1 and 2.

A possible alternative explanation to the hot plasma with a distribution of  $kT$  and  $\tau$  is Comptonisation by a plasma with nonthermal electron distribution. We have performed a number of Monte Carlo computations using either a Maxwellian electron distribution truncated at high energies or electron power-law distributions constrained to low values of the Lorentz factor ( $\lesssim 2$ ). Our conclusion is that those models can in principle provide high-energy cut-offs stronger than those from the Maxwellian. However,  $\chi^2$  fitting of Monte Carlo results would require a very extensive grid of models. Instead, an iterative-scattering method (PS96) modified for Comptonisation by a non-Maxwellian distribution appears to provide a simpler solution to this problem (J. Poutanen, private communication). We leave detailed investigation of this issue for future work.

### 3.2 Energy balance, geometry, and pair production

In Section 3.1 above, we have ruled out the disc-corona model for Cyg X-1 based on spectral fitting alone. This conclusion can be further supported by considering the energy balance between the hot and the cold phase.

The presence of Compton reflection shows there is cold matter in the vicinity of the  $X\gamma$  source. Only some of the incident  $X\gamma$  photons get reflected (with the integrated albedo of  $\sim 0.15$ , e.g., Magdziarz & Zdziarski 1995), but most

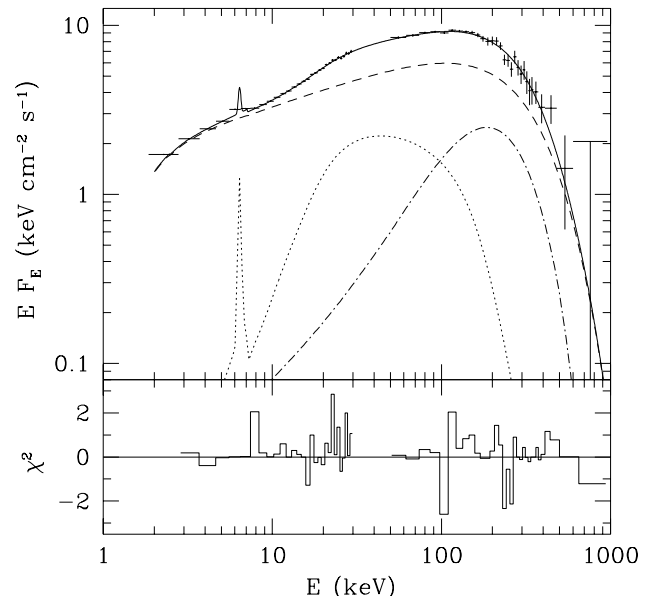


**Figure 4.** The two-temperature thermal Comptonisation fit to the data set 1. The dashed and dot-dashed curves represent the primary and secondary Comptonisation components, respectively. The dotted curve represents Compton reflection of the primary component. The solid curve gives the sum. This model provides a statistically satisfactory description of the data.

( $\sim 0.85$ ) are absorbed and reemitted in soft X-rays with a distribution close to a blackbody. Depending on the geometry, a fraction of the blackbody photons will return to the  $X\gamma$  source and provide some of the seeds for thermal Compton upscattering, which cools the hot plasma. (Further cooling can be provided by a blackbody flux from dissipation of gravitational energy in the cold matter). The ratio of the luminosity in the  $X\gamma$  spectrum to that of the seed photons (the Compton amplification factor) determines the

resultant spectral shape because, at a given optical depth, the electron temperature is determined by the amount of cooling photons incident on the hot plasma. From Monte-Carlo simulations, we find that the rather flat continuum spectrum ( $\alpha \sim 0.6$ ) extending out to  $\sim 150$  keV can only be produced if the incident seed photon luminosity is about 14 times less than the luminosity in the Comptonised  $X\gamma$  spectrum. This rules out a homogeneous disc-corona geometry of the source, in which approximately half of the hard X-ray photons are intercepted by the disc, 85 per cent of which are thermalised, and then re-intercepted by the corona, giving an X-ray luminosity only  $\sim 2.4$  times that of the seed photons. The lack of soft photons could in principle be obtained if the hot corona is in the form of detached active regions (e.g., PS96). However, this would imply an observed solid angle covered by the reflecting medium as seen from the hot source close to  $2\pi$  whereas the observed value is  $\sim 0.4 \times 2\pi$ . This means that the hot source does *not* form a corona (either homogeneous or patchy) above the surface of a cold disc, fully consistent with the results of spectral fitting in Section 3.1.

Assuming that the reflection spectrum is not strongly Comptonised, i.e., the observed amount of reflection is indicative of the solid angle subtended by the cold material to the hard X-ray source, then we can estimate the fraction,  $g$ , of the reprocessed radiation that returns to the hot source to form the Compton seed photons. From energy balance considerations  $g \leq (0.85 \times 0.5 \times \Omega/2\pi \times 14)^{-1} \simeq (6 \times \Omega/2\pi)^{-1} \sim 0.4$ . (A similar value was used in the fits in Section 3.1.) Again this highlights the problems of the homogeneous corona-disc geometry, in which all the reprocessed photons are re-intercepted by the hot plasma.

The considerations above explain the fit results in which we have been unable to obtain satisfactory models with the disc-corona model (see above). A possible source geometry consistent with the observed spectra is a hot inner region together with a colder outer disc (e.g. Shapiro, Lightman & Eardley 1976; Björnsson et al. 1996; Narayan 1996). This geometry explains the observed low reflection fraction, the large Compton amplification of seed photons, as well as the narrowness of the  $K\alpha$  line observed by E96. Also, the seed soft photons in this model are not produced underneath the hot plasma but rather come from various directions sideways. This then explains the absence of the anisotropy break in the spectrum. We intend to further investigate the expected spectrum from such geometry in future work.

The last issue we consider is the presence of  $e^\pm$  pairs in the hot source. Knowing the shape of the spectrum and  $\tau$  ( $\sim 1-2$ ), we can compute the compactness parameter,  $\ell \equiv L\sigma_T/Rm_e c^3$  (where  $R$  is the source size), at which photon-photon pair production rate is sufficient to produce pairs with the given  $\tau$  (Svensson 1984). We obtain  $\ell \sim 40-70$  roughly correlated with the luminosity varying in the range of  $\sim 0.02-0.03$  of the Eddington limit (assuming the mass of  $10M_\odot$ ). This implies an approximately constant lower limit on the source size of  $R \sim 5$  Schwarzschild radii. The source is pair-dominated at this limit, and is electron-dominated if  $R$  is much larger. The constancy with  $L$  is due to an approximate constancy of the model fluxes seen around 0.5 MeV (in spite of the overall  $X\gamma$  flux varying), see Figure 1.

We also note that the pair annihilation feature at the  $kT$  and  $\tau$  implied by the thermal Comptonisation model with

$e^\pm$  pairs would be rather weak, with the peak annihilation flux less than 0.1 of the observed 0.5 MeV flux (see Maciolek-Niedźwiecki, Zdziarski & Coppi 1995), and the luminosity in annihilation photons of less than  $\sim 2$  per cent of the total luminosity. Thus, the observed spectra are consistent with (but do not require) the hot ( $kT \sim 100$  keV) source made of  $e^\pm$  pairs.

Note that virtually all pair production is due to the hotter and optically thinner plasma component, with  $kT \simeq 100$  keV and  $\tau \sim 1-2$ . This can be seen in Figure 4, in which number of Wien photons around 0.5 MeV is much less than that in the main spectral component. Consequently, the cooler, optically thick, plasma ( $kT \simeq 50$  keV,  $\tau \sim 6$ ) is made entirely of electrons and protons.

## 4 CONCLUSIONS

We find the  $X\gamma$  source in Cyg X-1 does not form a corona above the surface of an accretion disc. Three arguments lead us to that conclusion: the solid angle subtended by the cold medium as seen from the  $X\gamma$  source is significantly smaller than  $2\pi$ , the  $X\gamma$  source is photon-starved, and there is no anisotropy break (necessary in the disc-corona models) in the X-ray spectrum. In addition, the reflecting cold medium is far away from the central black hole, as demonstrated by the narrowness of the fluorescent  $K\alpha$  line observed by *ASCA* (E96). All the properties above are consistent with a hot inner disc Comptonising soft photons from a cold outer disc. This distinguishes Cyg X-1 from some Seyfert 1s, in which the cold, reflecting, disc appears to extend all the way to the innermost stable orbit (e.g., Fabian et al. 1995). Note that this difference cannot be explained by the radiation-pressure disc instability in a disc-corona system, which is stronger for more massive black holes (e.g., Svensson & Zdziarski 1994).

The most likely radiative process producing  $X\gamma$  photons in Cyg X-1 is Comptonisation of seed soft X-rays photons. The observed sharpness of the high-energy cutoff rules out a uniform thermal plasma. Either a distribution of plasma parameters or an electron distribution different from a Maxwellian is required. A remarkable property of the spectra is their almost constant shape with the varying amplitude. In models with repeated Compton scattering, this implies the constancy of the plasma parameters (e.g.,  $\tau$  and  $kT$  for thermal Comptonisation) with changing accretion rate. This represents a strong constraint on future models of Cyg X-1. In particular, *simplest* thermal  $e^\pm$  pair models predict a strong dependence of  $\tau$  on the luminosity (e.g. Zdziarski 1985). The constant spectral shape can be achieved in models with high-energy nonthermal electrons (e.g., Svensson 1987; Lightman & Zdziarski 1987). However, these models predict a strong annihilation feature which is not seen in the data (P96), although this constraint could be possibly weakened if the annihilation rate were reduced by having the pairs reaccelerated before they lose energy completely.

## ACKNOWLEDGEMENTS

This research has been supported in part by the Polish KBN grants 2P03D01008 and 2P03D01410 and NASA grants and

contracts. We are grateful to Juri Poutanen for providing us with his disc-corona code and extensive discussions. We also thank Paweł Magdziarz for his assistance with implementing models into the XSPEC software package.

## REFERENCES

Anders E., Ebihara M., 1982, *Geochim. Cosmochim. Acta*, 46, 2363

Arnaud K. A., 1996, in: Jacoby G. H., Barnes J., eds., *Astronomical Data Analysis Software and Systems V*, ASP Conf. Series Vol. 101, San Francisco, p. 17

Balucińska-Church M., Belloni T., Church M. J., Hasinger G., 1995, *A&A*, 302, L5

Barr P., White, N. E., Page, C. G. 1985, *MNRAS*, 216, 65P

Björnsson G., Abramowicz M. A., Chen X., Lasota J.-P., 1996, *ApJ*, 467, 99

Bowyer, S., Byram, E. T., Chubb, T. A., Friedman, M., 1965, *Science*, 147, 394

Cui W., Heindl W. A., Rothschild R. E., Zhang S. N., Jahoda K., Focke W., 1997, *ApJ*, 474, L57

Dolan J. F. 1992, *ApJ*, 384, 249

Dolan J. F., Tapia S., 1989, *ApJ*, 344, 830

Done C., Mulchaey J. S., Mushotzky R. F., Arnaud K. A., 1992, *ApJ*, 395, 275

Ebisawa K., Ueda Y., Inoue H., Tanaka Y., White N. E., 1996, *ApJ*, 467, 419 (E96)

Fabian A. C., Nandra K., Reynolds C. S., Brandt W. N., Otani C., Tanaka Y., 1995, *MNRAS*, 277, L11

George I. M., Fabian A. C., 1991, *MNRAS*, 249, 352

Gies D. R., Bolton C. T., 1986, *ApJ*, 304, 371

Haardt F., 1993, *ApJ*, 413, 680

Haardt F., Done C., Matt G., Fabian A. C., 1993, *ApJ*, 411, L95

Haardt F., Maraschi L., 1993, *ApJ*, 413, 507

Kaastra J. S., Mewe R., 1993, *A&AS*, 97, 443

Kitamoto S., Miyamoto S., Tanaka Y., Ohashi T., Kondo Y., Tawara Y., Nakagawa M., 1984, *PASJ*, 36, 731

Lampton M., Margon B., Bowyer S., 1976, *ApJ*, 208, 177

Liang E. P., Nolan P. L., 1984, *Space Sci. Rev.*, 38, 353

Lightman A. P., Zdziarski A. A., 1987, *ApJ*, 319, 643

Maciołek-Niedźwiecki A., Zdziarski A. A., Coppi P. S., 1995, *MNRAS*, 276, 273

Magdziarz P., Zdziarski A. A., 1995, *MNRAS*, 273, 837

Marshall F. E., Mushotzky R. F., Petre R., Serlemitsos P. J., 1993, *ApJ*, 419, 301

Misra R., Melia F., 1996, *ApJ*, 467, 405

Miyamoto S., Kitamoto S., 1989, *Nature*, 342, 773

Narayan R., 1996, *ApJ*, 462, 136

Phlips B. F., et al., 1996, *ApJ*, 465, 907 (P96)

Poutanen J., Svensson R., 1996, *ApJ*, 470, 249 (PS96)

Priedhorsky W. C., Terrel J., Holt S. S., 1983, *ApJ*, 270, 233

Reilman R. F., Manson S. T., 1979, *ApJS*, 40, 815

Shapiro S. L., Lightman A. P., Eardley D. M., 1976, *ApJ*, 204, 187

Stern B. E., Poutanen J., Svensson R., Sikora M., Begelman M. C., 1995, *ApJ*, 449, L13

Sunyaev R. A., Trümper J., 1979, *Nature*, 279, 506

Svensson R., 1984, *MNRAS*, 209, 175

Svensson R., 1987, *MNRAS*, 227, 403

Svensson R., 1996, *A&AS*, 120, 475

Svensson R., Zdziarski A. A., 1994, *ApJ*, 436, 599

Turner M. J. L., et al., 1989, *PASJ*, 41, 345

Zdziarski A. A., 1985, *ApJ*, 289, 514

Zdziarski A. A., Johnson W. N., Magdziarz P., 1996, *MNRAS*, 283, 193